Thin Solid Films 534 (2013) 659–665

Contents lists available at SciVerse ScienceDirect

Thin Solid Films

journal homepage: www.elsevier.com/locate/tsf

Growth and characterization of topological insulator Bi_2Se_3 thin films on $SrTiO_3$ using pulsed laser deposition

Phuoc Huu Le [a], Kaung Hsiung Wu [b], Chih Wei Luo [b,1], Jihperng Leu [a,*]

[a] Department of Materials Science and Engineering, National Chiao Tung University, Hsinchu 30049, Taiwan, ROC
[b] Department of Electrophysics, National Chiao Tung University, Hsinchu 30049, Taiwan, ROC

ARTICLE INFO

Article history:
Received 29 June 2012
Received in revised form 24 January 2013
Accepted 25 January 2013
Available online 4 February 2013

Keywords:
Bi_2Se_3
Topological insulator
Thin film
Pulsed laser deposition
$SrTiO_3$ substrate

ABSTRACT

Bismuth selenide (Bi_2Se_3) thin films were grown on $SrTiO_3$(111) (STO) substrates using pulsed laser deposition (PLD). The structural, morphological, electrical, and transport properties were studied at various substrate temperatures (T_S) from 120 to 350 °C. Amorphous films grown at $T_S<180$ °C exhibited semiconducting behavior, and highly c-axis-oriented textured films deposited at $T_S\geq180$ °C exhibited metallic behavior. Bi_2Se_3 thin-films were epitaxially grown on STO substrates at 300 and 350 °C. Thickness-dependent characteristics were also investigated for optimized Bi_2Se_3 films deposited at $T_S=230$ °C. The semiconducting or metallic characteristics of Bi_2Se_3 films prepared using PLD were observed through electrical and transport results.

© 2013 Elsevier B.V. All rights reserved.

1. Introduction

Topological insulators (TIs) are quantum matter with the bulk band-gap of an ordinary insulator, but possess one or more robust metallic surface states, protected by time-reversal symmetry due to strong spin–orbit coupling [1–4]. Bi_2Se_3 is one of the best TIs because it has a gapless single Dirac cone and a bulk band-gap (approximately 300 meV) that is larger than other comparable materials, such as Bi_2Te_3 (165 meV) [5] and Sb_2Te_3 (250–300 meV) [5,6]. When this material is grown, it tends to form selenium (Se) vacancies or antisites that serve as donors and further shift the Fermi energy considerably above the band gap [5,7,8]. These doped electrons in the conduction band create difficulties when detecting Dirac-cone surface states during transport measurements. To overcome this high electron-doping problem, a Se-rich environment is created during growth or doping with Ca, Cu, or Sn to prepare stoichiometric Bi_2Se_3 thin-films [9–11]. For example, in molecular beam epitaxy (MBE) deposition, a Se-rich environment can be created by controlling the Se:Bi flux ratio (typically ranging from 10:1 to 30:1) [3,12,13]. Compared to MBE deposition, PLD offers advantages, such as a higher instantaneous deposition rate, relatively high reproducibility, and low costs.

Few studies have examined Bi_2Se_3 thin-films deposited using PLD. Onose et al. [14] successfully grew epitaxial Bi_2Se_3 thin-films on InP(111) substrates using a designed target with an atomic ratio of Bi: Se of 2:8. Meng et al. [15] also reported the PLD deposition of Bi_2Se_3 thin-films on Si(100) substrates using an alloy target.

This study uses STO as a substrate because of its lower lattice mismatch (5.8%) for Bi_2Se_3 (7.9% for silicon substrates and 13% for sapphire substrates). C-axis Bi_2Se_3 thin-films were successfully grown on STO substrates using PLD and a stoichiometric polycrystalline Bi_2Se_3 target. STO is an insulating substrate; therefore, substrate conductance can be ignored for electrical transport studies. This study investigates the effects of T_S and thickness on the structural, morphological, compositional, and electrical properties of c-axis Bi_2Se_3 thin-films. The results of this study provide a comprehensive understanding of the optimal growth conditions for Bi_2Se_3 thin-films, using the relatively economical and simple PLD technique, which could be used to prepare highly c-axis-oriented TI thin-films for further research and applications.

2. Experimental details

Bi_2Se_3 thin-films were deposited on STO (111) substrates using PLD. Ultra-violet pulses (duration 20 ns) from a KrF excimer laser ($\lambda=248$ nm, 2 Hz repetition) were focused on a stoichiometric polycrystalline Bi_2Se_3 target with a pulse fluence of 3.7 J/cm^2. The target-to-substrate distance (d_{T-S}) was 40 mm. The base pressure remained better than 0.4 mPa (or 3×10^{-6} Torr). Helium (He)—with a pressure of 40 Pa (300 mTorr)—was used to produce plasma to assist deposition. Before deposition, the STO substrate was cleaned using acetone, methanol, and de-ionized water in an ultrasonic cleaner for 30 min to remove organic contaminants. Bi_2Se_3 thin-films were

* Corresponding author. Tel.: +886 35131420; fax: +886-3-5724727
E-mail addresses: cwluo@mail.nctu.edu.tw (C.W. Luo), jimleu@mail.nctu.edu.tw (J. Leu).
[1] Tel.: +886 35712121 56196.

0040-6090/$ – see front matter © 2013 Elsevier B.V. All rights reserved.
http://dx.doi.org/10.1016/j.tsf.2013.01.104

deposited at T_S between 120 and 350 °C and a deposition time of 7 min for the temperature-dependent study. For the thickness-dependent study, films between 30 and 1200 nm thick were prepared at deposition times from 1 to 45 min at a certain optimized T_S. The average growth rate was approximately 30 nm/min (at 230 °C).

The orientation and crystallinity of the Bi_2Se_3 thin-films were determined using X-ray diffraction (XRD; Bruker D8) with CuK_α radiation ($\lambda = 1.54$ Å) in $2\theta-\omega$ and ϕ-scan configurations. Digital images from a high-resolution transmission electron microscope (HRTEM; Philips Tecnai F20) operated at 200 kV were recorded using a Gatan 2k×2k CCD camera system to obtain detailed film-structure information. The HRTEM specimens were prepared using a standard mechanical thinning and Ar ion milling procedure. The chemical stoichiometry of the Bi_2Se_3 thin-films was characterized using X-ray photoelectron spectroscopy (XPS; ThermoVG 350) with the X-ray source (MgK_α 1253.6 eV, 300 W). The binding energies obtained in the XPS analysis were standardized using C1s at 284.6 eV. XPS curve fitting was performed using the freeware XPSPEAK 4.1, the Shirley background subtraction, and assuming a Gaussian–Lorentzian peak shape. Raman spectra were collected using an NT-MDT confocal Raman microscopic system with a laser wavelength of 473 nm and a laser spot size of approximately 0.4 μm. The Si peak at 520 cm^{-1} was used as a reference for wavenumber calibration. The morphology of the Bi_2Se_3 thin-films was characterized using atomic force microscopy (AFM; Veeco Escope). The film compositions and thicknesses were examined using energy dispersive X-ray spectroscopy (EDX; Oxford Instruments) and field-emission scanning electron microscopy (FE-SEM; JEOL JSM-6500), respectively. The operating conditions for EDX measurements were an accelerating voltage of 15 kV, an elevation angle of 35°, a dead time around 25–30%, and a collecting time of 90s. The resistivity, carrier mobility, and concentration were measured at room temperature using a Hall effect measurement system (Bio-Rad HL5500PC) with van der Pauw geometry. Indium balls were used to achieve better ohmic contact on the surface of the Bi_2Se_3 thin-films. The temperature-dependent resistances of the Bi_2Se_3 films, $R(T)$, were measured using a standard four-point probe method from room temperature to 20 K.

3. Results and discussions

Fig. 1(a) shows the XRD patterns of Bi_2Se_3 thin-films deposited at T_S from 120 to 350 °C. In the 120 and 150 °C cases, only peaks attributable to the substrate are present, indicating that the films are amorphous. When the deposition temperature increased to 180 °C and above, the deposited films became polycrystalline with a highly c-axis-preferred orientation (textured films). The crystallinity of the Bi_2Se_3 thin-films increased with increasing T_S, as shown by the increasing intensity and decreasing full width at half maximum (FWHM) of diffraction peaks, such as (003), (006), (009), and (0015). Specifically, the FWHM of the (006) peak decreased from 0.89° to 0.18° as T_S increased from 180 to 350 °C, as shown in Fig. 1(b).

HRTEM was performed on a 200-nm-thick Bi_2Se_3 film deposited at 230 °C to examine the film-structure quality, as shown in Fig. 1(c). The projected periods of 9.60 and 4.80 Å along the c-axis correspond to the lattice spacing of the (003) and (006) planes, respectively. The

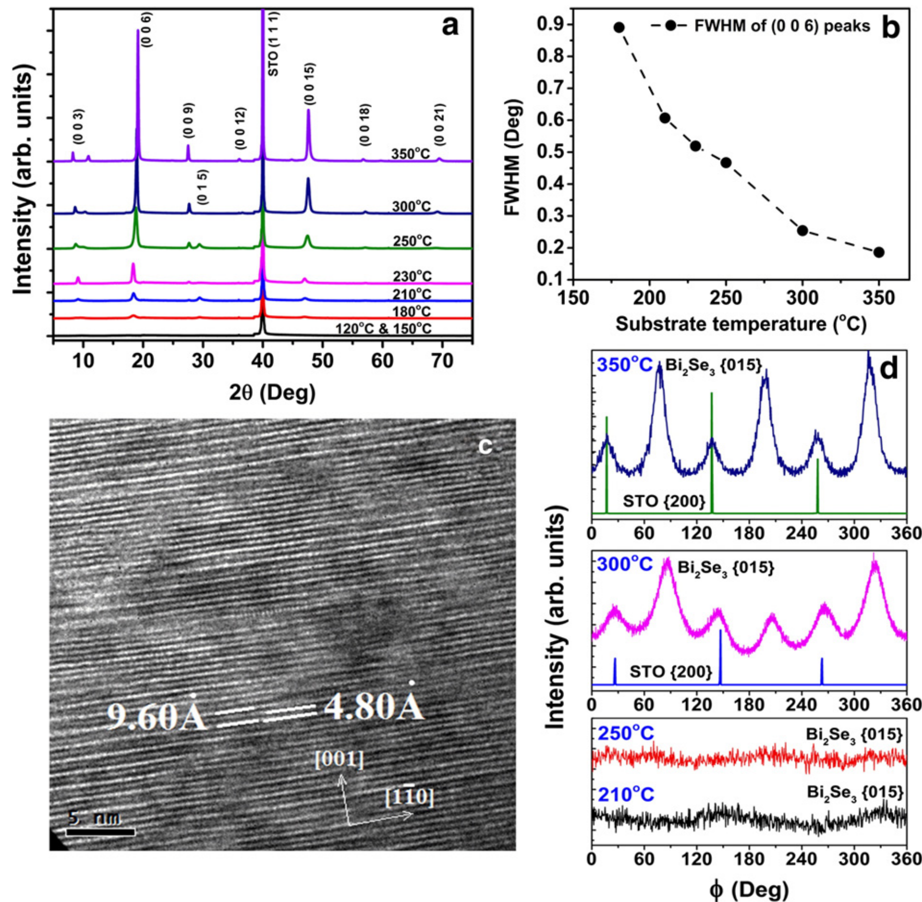

Fig. 1. (a) $2\theta-\omega$ X-ray diffraction patterns of 200-nm-thick Bi_2Se_3 films deposited at substrate temperatures from 120 to 350 °C. (b) FWHM of the (006) peaks as a function of deposition temperatures. (c) A HRTEM cross-sectional image of a 200-nm-thick Bi_2Se_3 film deposited at 230 °C. (d) The XRD ϕ-scan patterns of STO (200) plane and Bi_2Se_3 (015) plane that were grown at 210, 250, 300, and 350 °C.

parallel lattice planes are also perpendicular to the [001] direction, reflecting the c-direction film ordering. For the hexagonal Bi_2Se_3 unit cell, the lattice parameters are expressed using Eq. (1).

$$\frac{1}{d_{hkl}^2} = \frac{4}{3}\left(\frac{h^2+hk+k^2}{a^2}\right) + \frac{\ell^2}{c^2}. \quad (1)$$

The c-axis lattice constant of the film is 28.80 Å, which is consistent with that of a single crystal (28.64 Å) [16]. The film c-axis lattice constant is slightly larger than that of single crystal because of a substrate-film lattice mismatch. Because $a_{STO} = 3.9$ Å $< a_{Bi2Se3} = 4.14$ Å, the mismatch can cause biaxial compressive strain, increasing the film c-axis lattice constant.

Fig. 1(d) shows the ϕ-scan patterns of Bi_2Se_3 films deposited on STO (111) at various T_S measured at a tilt angle (χ) of 57.9°, which corresponds to Bi_2Se_3 (015). Films deposited at 210 and 250 °C did not show any diffraction peaks, reflecting their in-plane polycrystalline characteristics. By contrast, films deposited at 300 and 350 °C exhibited the expected six-fold symmetric diffraction pattern for the

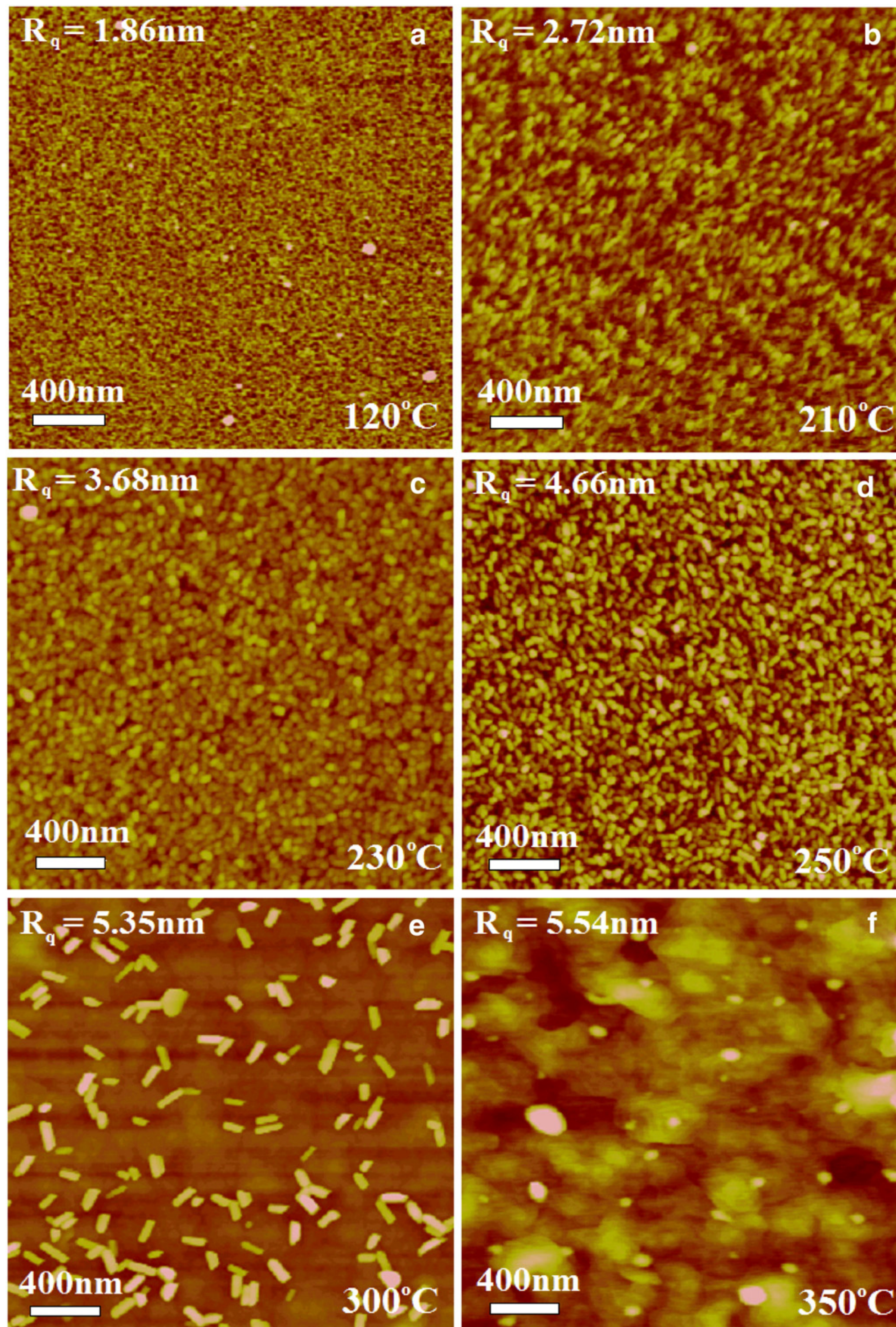

Fig. 2. AFM images of Bi_2Se_3 films deposited at various substrate temperatures from 120 to 350 °C: (a) 120 °C, (b) 210 °C, (c) 230 °C, (d) 250 °C, (e) 300 °C, and (f) 350 °C.

{015} [17,18] and grew epitaxially on the STO substrates. The epitaxial relationship between film and substrate is Bi_2Se_3(001)//STO(111) and Bi_2Se_3[110]//STO $\left[\bar{1}10\right]$. This was determined by comparing Bi_2Se_3{015} and STO{200} diffraction peaks. The T_S-dependent in-plane characteristic suggests that $T_S \leq 250$ °C is insufficient for atomic migration and for establishing an epitaxial film–substrate interface.

Fig. 2(a)–(f) shows the surface morphology and roughness evolution of Bi_2Se_3 thin-films (approximately 200 nm) deposited at T_S from 120 to 350 °C. The films had relatively smooth surfaces with a root-mean-square roughness (R_q) between 1.86 and 5.54 nm. Film roughness increased as T_S increased. Bi_2Se_3 thin-films deposited at $120 \leq T_S \leq 250$ °C exhibited densely packed islands with polycrystalline morphology. At $T_S = 300$ °C, the film exhibited a roughness of 5.35 nm with random precipitations. These were probably caused by a Bi-rich phase [18]. At 350 °C, the film showed step-and-terrace structures and a maximal roughness of 5.54 nm.

To assess film chemical stoichiometry and purity, ex situ XPS characterization of Bi_2Se_3 film deposited at 230 °C was performed. The full-range scan in Fig. 3(a) shows the major Bi and Se peaks and relatively small peaks of O and C. The presence of carbon and oxygen related adspecies is likely due to surface hydrocarbon contaminants and moisture uptake [19]. The Se 3d spectrum in Fig. 3(b) can be fitted perfectly using the two peaks for Se $3d_{5/2}$ and $3d_{3/2}$ with binding energies of 53.5 and 54.1 eV, respectively [15,20]. This implies that Se exists in the films as a Bi_2Se_3 compound. The Bi 4f spectrum shown in Fig. 3(c) can be fitted with the Bi $4f_{7/2}$ and $4f_{5/2}$ peaks at 158.1 and 163.4 eV, respectively [20]. The binding energy of the Se $3d_{5/2}$ peak shows a red shift (approximately 2.2 eV), compared with that of pure bulk Se, and the binding energies of the Bi 4f peaks show a blue shift (approximately 1.1 eV). Se–Bi bonding causes opposite shifts in binding energy, where the charge transfers from Bi to Se [20,21]. This confirms the formation of high-purity Bi_2Se_3 films found in this study. The excellent chemical stoichiometry of films deposited at T_S from 210 to 250 °C is shown in the EDX results in Fig. 4(b). The atomic ratio of Bi:Se was close to 2:3, confirming that the Bi_2Se_3 phase was present in the thin films. Raman spectroscopy also confirmed the existence of the Bi_2Se_3 phase. Fig. 3(d) shows a typical Raman spectrum of a 200-nm-thick Bi_2Se_3 film deposited at 230 °C. Two characteristic peaks occur at 131.5 and 174.5 cm^{-1}, which are associated with the E_g^2 and A_{1g}^2 vibrational modes in Bi_2Se_3 single crystals, respectively [22]. The A_{1g}^1 mode (at 72 cm^{-1}) is beyond the measurable range (>100 cm^{-1}) of the Raman spectrometer [22].

The electrical properties (resistivity (ρ), carrier mobility and carrier concentration) of 200-nm-thick Bi_2Se_3 films deposited at various T_S are shown in Fig. 4(a). The room-temperature resistivity of Bi_2Se_3 films decreased as T_S increased from 120 to 300 °C and became constant at $T_S \geq 300$ °C. Meng et al. [15] also noted this phenomenon. When T_S increased from 120 to 180 °C, film carrier concentration significantly decreased because of fewer defects. This is probably because antisite defects dominate at such high carrier concentrations and low T_S deposition levels. This is reasonable because an excess of Se (over the dashed line of the stoichiometric Se concentration) is observed in the low temperature region (≤210 °C) in Fig. 4(b). The atoms do not have sufficient energy to move and locate their lowest potential-energy sites in a low-temperature growth regime; therefore the excess Se is more likely to occupy the Bi sites and acts as an n-type dopant. This is similar to the findings for Bi_2Te_3 films grown by MBE deposition [23], where the Te_{Bi} antisite dominates and acts as a

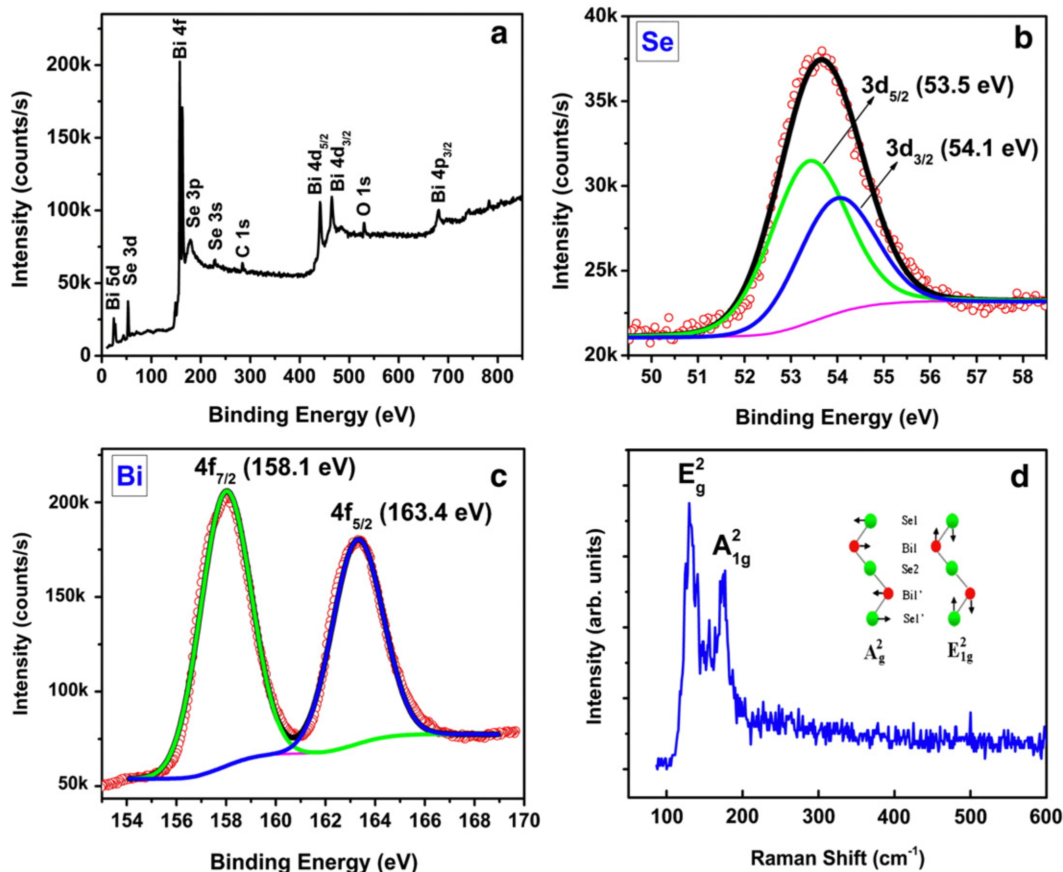

Fig. 3. (a) Wide-scan XPS spectra of a 200-nm-thick Bi_2Se_3 film deposited at 230 °C. XPS spectra of (b) Se 3d and (c) Bi 4f (the solid lines are the fitting curves). (d) Raman spectrum with excitation light of 473 nm.

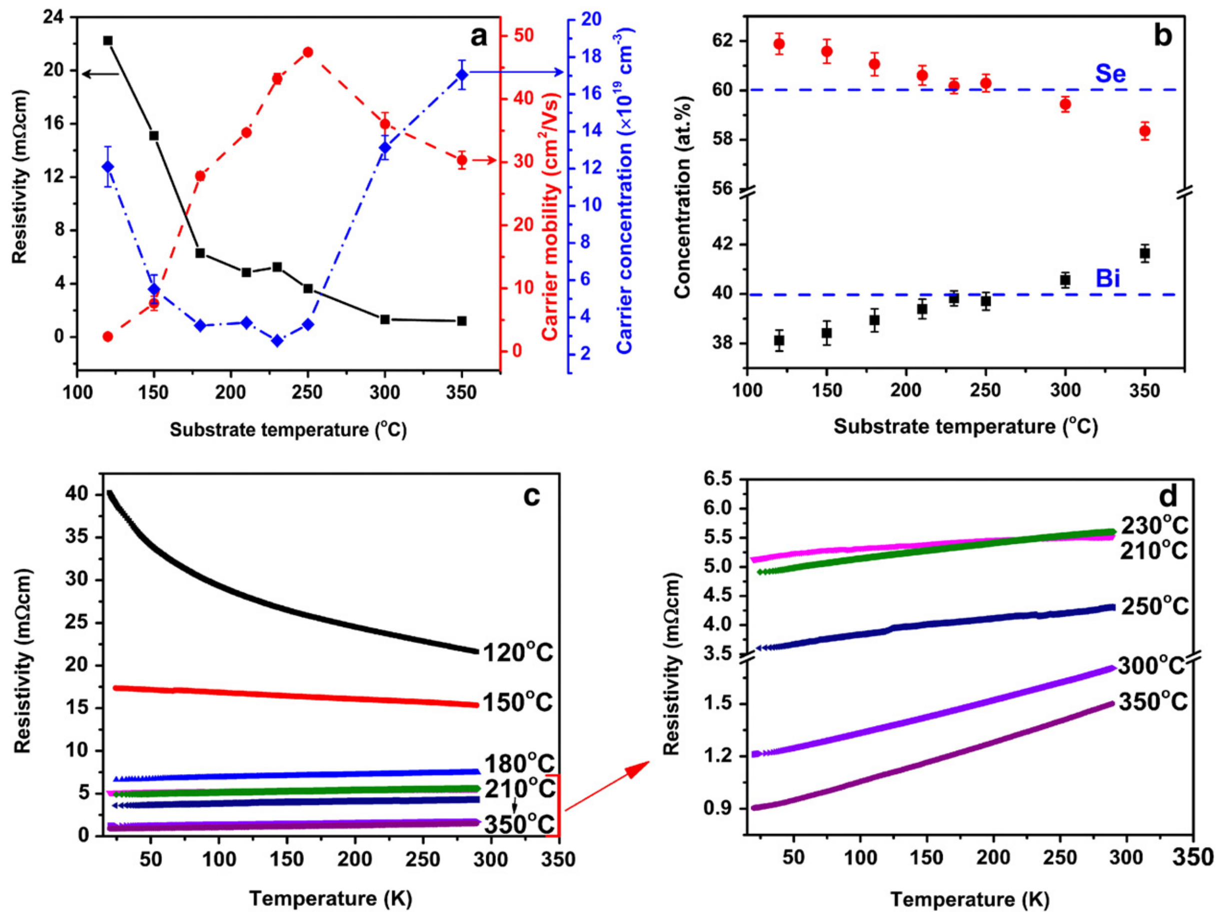

Fig. 4. Substrate temperature-dependent (a) resistivity, carrier mobility and carrier concentration, (b) Bi and Se concentrations (dotted lines correspond to the stoichiometric composition) in Bi_2Se_3 films. (c) Temperature-dependent resistivities of Bi_2Se_3 films deposited at various substrate temperatures. (d) The zoomed-in view of the Bi_2Se_3 films grown at substrate temperatures from 210 to 350 °C.

dopant because the formation energy of the Te_{Bi} antisite is lower than that of the Bi_{Te} antisite or Te vacancy in a Te-rich environment at low T_S. From 180 to 250 °C, carrier concentration is relatively low, with an average value of 3.4×10^{19} cm^{-3}. This is attributed to the minimization of antisite defects and Se vacancies because of the slightly Se-rich environment (i.e., the small deviation from the stoichiometric Bi:Se ratio in a moderate temperature range), as shown in Fig. 4(b). By contrast, the carrier mobility monotonically and dramatically increases from 120 to 250 °C because of the reduction in grain-boundary scattering from larger grains, as shown by the AFM images in Fig. 2(a)–(d).

At 230 °C, carrier concentration reached a minimal value of 2.75×10^{19} cm^{-3} (slightly higher than 2.1×10^{19} cm^{-3} in [14]) and mobility achieved a high value of 43.2 cm^2 V^{-1} s^{-1}. After reaching the highest value of 47.4 cm^2 V^{-1} s^{-1} at 250 °C, mobility decreased slightly because carrier concentration gradually increases (as expected) in semiconductor materials. When T_S increased from 250 to 350 °C, Se concentration decreased slightly because a portion of the selenium transformed into the Se_2 gas phase during deposition because Se vapor pressure is higher than Bi vapor pressure [24]. Thus, Se vacancies are more likely to form [25] in Bi_2Se_3 films grown at $T_S\geq250$ °C.

Similar electrical characteristics were reported for Bi_2Te_3 films grown by co-sputtering [26]. For Bi_2Se_3 films prepared by PLD, this study's carrier concentration and mobility results differ from those reported in Ref. [15]. In this study, the carrier mobility (carrier concentration) of the Bi_2Se_3 film deposited at 210 °C was approximately 34.7 cm^2 V^{-1} s^{-1} (3.7×10^{19} cm^{-3}), which is considerably higher (lower) than approximately 6 cm^{2}V^{-1} s^{-1} (2.3×10^{21} cm^{-3}) for the Bi_2Se_3 film deposited at 200 °C, reported by Meng et al. [15]. This high carrier mobility may be caused by decreased scatterings, such as ionized impurity and grain boundary scatterings, or the partial contribution of surface state carriers when the films become polycrystalline with a c-axis orientation at $T_S\geq180$ °C.

Fig. 4(c) and (d) show the temperature-dependent resistivity of films deposited at various T_S. For amorphous films grown at 120 and 150 °C, resistivity increased as temperature decreased ($d\rho/dT<0$), a typical behavior for semiconductors because these films have an amorphous structure. However, the temperature-dependent resistivity of textured films deposited at $T_S\geq180$ °C clearly demonstrated a metallic tendency ($d\rho/dT>0$). Degenerate doping of semiconductors can cause metallic conductivity ($d\rho/dT>0$). For Bi_2Se_3 films, selenium vacancies are the main defects which cause electron doping up to 10^{19} cm^{-3}. Therefore, textured films should exhibit metallic behavior, which makes distinguishing metallic surface states from metallic bulk states using transport properties difficult. However, the contribution of surface state in textured films deposited at $T_S\geq180$ °C is expected for polycrystalline Bi_2Te_3 and Sb_2Te_3 thin-films [27] and for c-axis-oriented Bi_2Se_3 thin-films deposited by PLD [28]. A temperature of 230 °C is the optimal T_S for growing Bi_2Se_3 thin-film on STO (111) substrate using PLD. This T_S produces film with the lowest carrier concentration, high carrier mobility, excellent atomic stoichiometry, metallic behavior, a relatively good c-axis-textured structure, and a smooth surface morphology ($R_q=3.68$ nm).

Because bulk and surface transport properties demonstrate different thickness dependencies, thickness-dependent transport studies can provide insight into bulk and surface states. This study prepared a series of Bi_2Se_3 films with thicknesses ranging from 30 to 1200 nm at the

optimal temperature of 230 °C. Fig. 5(a) shows that the carrier mobility increases considerably and sheet resistance monotonically decreases when film thickness increases, becoming constant at approximately 300 nm. The thickness-dependent mobility is described by Eq. (2) [29]:

$$\mu(t) = \mu_\infty/(1+2(\lambda/t)(1-p)), \quad (2)$$

where μ_∞ is the carrier mobility in a film in which the thickness t is substantially larger than the mean free path λ, and p represents the fraction of the carriers reflected specularly from the surface (the dashed line in Fig. 5(a)). The fitting yields of $\mu_\infty = 34.5 \pm 0.7$ cm^2/V s and $\lambda(1-p) = 8.5 \pm 1.7$ nm, conflict with the experimental values of 3000 cm^2/V s and 70 nm obtained in [30] because the higher average carrier concentration of 7.8×10^{19} cm^{-3} in the films in this study suppresses the carrier mobility and mean free path. This carrier mobility increase could also be caused by reduced grain boundary scattering from the grain-growth effect in thicker films deposited at 230 °C.

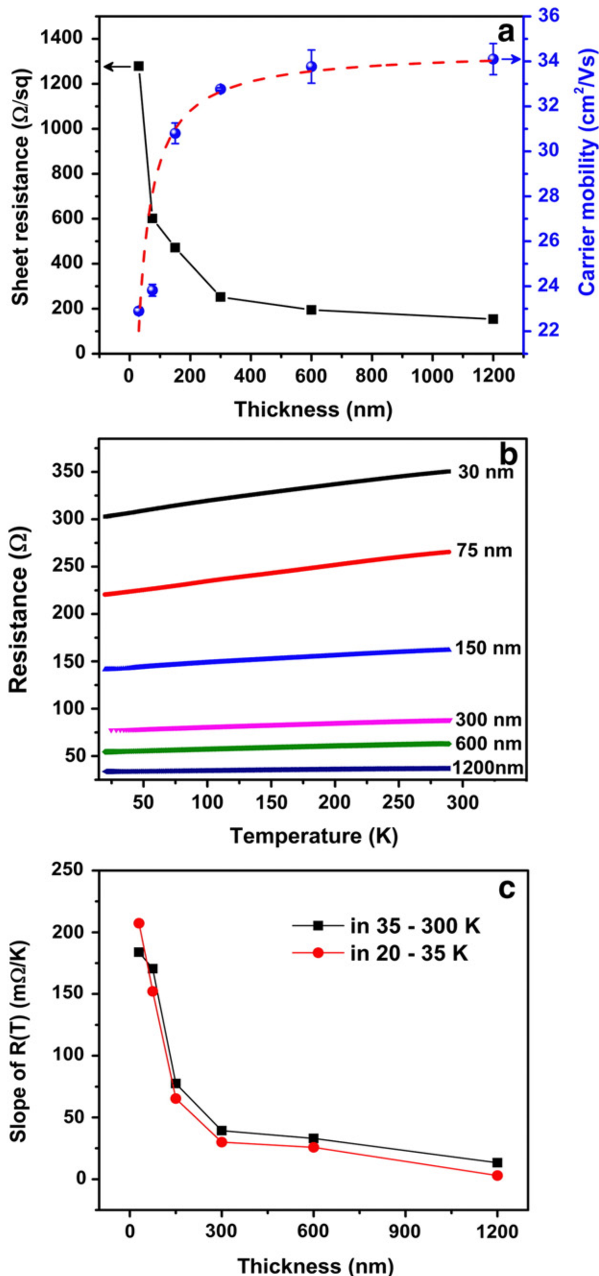

Fig. 5. (a) Thickness-dependent sheet resistance and carrier mobility of the Bi_2Se_3 films grown at 230 °C. The dashed line is the fitting result. (b) Temperature-dependent resistance of the Bi_2Se_3 films grown at 230 °C with various thicknesses from 30 to 1200 nm. (c) The slope of $R(T)$ curves (in (b), obtained from linear fitting) vs. film thickness in two temperature ranges of 35–300 K (solid square) and 20–35 K (solid circle).

Fig. 5(b) shows that all temperature-dependent resistances of Bi_2Se_3 films of various thicknesses are metallic. At room temperature, resistance decreased as thickness increased, which is consistent with the results in Ref. [14]. The slope of the $R(T)$ curves, $|dR/dT|$, from linear fitting in 35–300 K and 20–35 K ranges systematically decreased with increasing film thickness as shown in Fig. 5(c). At certain thicknesses (except for 30 nm), the slope in the lower temperature range is smaller than in the higher range, indicating weak localization of electrons [14]. Unfortunately, the domination of the degenerated semiconducting bulk state in Bi_2Se_3 films may totally conceal the contribution of the surface state in $R(T)$ when bulk and surface states simultaneously appear. This means that the $R(T)$ slope difference mainly relies on the change in bulk carrier mobility and concentration with temperature, which should be affected by the intrinsic internal quality of films deposited at various thicknesses.

4. Conclusions

Bi_2Se_3 thin-films were prepared on STO (111) substrates using PLD. The effects of substrate temperature (120 to 350 °C) and film thickness (30 to 1200 nm) on the electrical and material characteristics of Bi_2Se_3 thin-films were systematically investigated. The temperature-dependence study showed that amorphous films with low mobility and semiconducting behavior can be prepared at $T_S < 180$ °C and that highly c-axis-textured films with higher mobility and metallic behavior can be grown at $T_S \geq 180$ °C. Films grown at $180 \leq T_S \leq 250$ °C exhibited polycrystalline in-plane characteristics and films deposited at 300 and 350 °C were grown epitaxially on the STO substrates. The optimal deposition temperature for growing Bi_2Se_3 thin-films on STO (111) was 230 °C, because it produced the lowest carrier concentration of 2.75×10^{19} cm^{-3}, a high mobility of 43.2 cm^2 V^{-1} s^{-1}, a smooth morphology with $R_q = 3.68$ nm, and excellent atomic stoichiometry. The thickness-dependence study of Bi_2Se_3 films-deposited at 230 °C showed that mobility increased, sheet resistance decreased, and the slope of metallic $R(T)$ curves systematically decreased with increasing film thickness. However, information from the metallic surface state could not be extracted from the $R(T)$ results because of degenerate semiconducting bulk doping, which also exhibits metallic behavior. To overcome this limitation, film quality should be improved by minimizing native defects.

Acknowledgments

We are thankful to Mr. Q.H. Nguyen, Mr. T.T. Vu for the help with TEM and AFM measurements. One of the authors (P.H. Le) is thankful to Prof. J. Y. Juang, Prof. J.-Y. Lin, Prof. T. M. Uen for the support of using equipments and Mr. Y.-J. Chen, Mr. H.-J. Chen, Mr. H.J. Wang for the useful discussions. Financial support from the National Science Council of the Republic of China (Taiwan) under contract nos.: NSC 100-3113-E-007-001, NSC 101-3113-E-007-001, and NSC 101-2112-M-009-016-MY2, is gratefully acknowledged.

References

[1] D. Hsieh, D. Qian, L. Wray, Y. Xia, Y.S. Hor, R.J. Cava, M.Z. Hasan, Nature 452 (2008) 970.
[2] M.Z. Hasan, C.L. Kane, Rev. Mod. Phys. 82 (2010) 3045.
[3] A. Richardella, D.M. Zhang, J.S. Lee, A. Koser, D.W. Rench, A.L. Yeats, B.B. Buckley, D.D. Awschalom, N. Samarth, Appl. Phys. Lett. 97 (2010) 262104.
[4] A.D. LaForge, A. Frenzel, B.C. Pursley, T. Lin, X. Liu, J. Shi, D.N. Basov, Phys. Rev. B 81 (2010) 125120.
[5] Y.L. Chen, J.G. Analytis, J.H. Chu, Z.K. Liu, S.K. Mo, X.L. Qi, H.J. Zhang, D.H. Lu, X. Dai, Z. Fang, S.C. Zhang, I.R. Fisher, Z. Hussain, Z.X. Shen, Science 325 (2009) 178.
[6] H. Scherrer, S. Scherrer, in: D.M. Rowe (Ed.), CRC Press, Boca Raton, FL, 1995 Chap. 19.

[7] J. Navrátil, J. Horák, T. Plecháček, S. Kamba, J. Solid State Chem. 177 (2004) 1704.
[8] Y. Xia, D. Qian, D. Hsieh, L. Wray, A. Pal, H. Lin, A. Bansil, D. Grauer, Y.S. Hor, R.J. Cava, M.Z. Hasan, Nat. Phys. 5 (2009) 398.
[9] Y. Hor, A. Richardella, P. Roushan, Y. Xia, J.G. Checkelsky, A. Yazdani, M.Z. Hasan, N.P. Ong, R.J. Cava, Phys. Rev. B 79 (2009) 195208.
[10] Y.L. Wang, Y. Xu, Y.P. Jiang, J.W. Liu, C.Z. Chang, M. Chen, Z. Li, C.L. Song, L.L. Wang, K. He, X. Chen, W.H. Duan, Q.K. Xue, X.C. Ma, Phys. Rev. B 84 (2011) 075335.
[11] H.B. Zhang, H.L. Yu, D.H. Bao, S.W. Li, C.X. Wang, G.W. Yang, Adv. Mater. 24 (2012) 132.
[12] H.D. Li, Z.Y. Wang, X. Kan, X. Guo, H.T. He, Z. Wang, J.N. Wang, T.L. Wong, N. Wang, M.H. Xie, New J. Phys. 12 (2010) 103038.
[13] X. Chen, X.C. Ma, K. He, J.F. Jia, Q.K. Xue, Adv. Mater. 23 (2011) 1162.
[14] Y. Onose, R. Yoshimi, A. Tsukazaki, H. Yuan, T. Hidaka, Y. Iwasa, M. Kawasaki, Y. Tokura, Appl. Phys. Express 4 (2011) 083001.
[15] L. Meng, H. Meng, W. Gong, W. Liu, Z. Zhang, Thin Solid Films 519 (2011) 7627.
[16] W. Zhang, R. Yu, H.J. Zhang, X. Dai, Z. Fang, New J. Phys. 12 (2010) 065013.
[17] J.E. Brom, Y. Ke, R. Du, D. Won, X. Weng, K. Andre, J.C. Gagnon, S.E. Mohney, Q. Li, K. Chen, X.X. Xi, J.M. Redwing, Appl. Phys. Lett. 100 (2012) 162110.
[18] P. Tabor, C. Keenan, S. Urazdhin, D. Lederman, Appl. Phys. Lett. 99 (2011) 013111.
[19] X. Yang, X. Wang, Z. Zhang, J. Cryst. Growth 276 (2005) 566.
[20] G. Zhang, H. Qin, J. Teng, J. Guo, Q. Guo, X. Dai, Z. Fang, K. Wu, Appl. Phys. Lett. 95 (2009) 053114.
[21] J.H. Jeon, W.J. Jang, J.K. Yoon, Nanotechnology 22 (2011) 465602.
[22] W. Richter, H. Kohler, C.R. Becker, Phys. Status Solidi B 84 (1977) 619.
[23] G. Wang, X.G. Zhu, Y.Y. Sun, Y.Y. Li, T. Zhang, J. Wen, X. Chen, K. He, L.L. Wang, X.C. Ma, J.F. Jia, S.B. Zhang, Q.K. Xue, Adv. Mater. 23 (2011) 2929.
[24] H. Noro, K. Sato, H. Kagechika, J. Appl. Phys. 73 (1993) 1252.
[25] Z. Ren, A.A. Taskin, S. Sasaki, K. Segawa, Y. Ando, Phys. Rev. B 84 (2011) 075316.
[26] D.H. Kim, E. Byon, G.H. Lee, S. Cho, Thin Solid Films 510 (2006) 148.
[27] H.B. Zhang, H.L. Yu, G.W. Yang, EPL 95 (2011) 56002.
[28] G. Koren, T. Kirzhner, E. Lahoud, K.B. Chashka, A. Kanigel, Phys. Rev. B 84 (2011) 224521.
[29] A. Elshabini, F.D. Barlow, McGraw-Hill, New York, 1998, p. 4.
[30] Y.S. Kim, M. Brahlek, N. Bansal, E. Edrey, G. Kapilevich, K. Iida, M. Tanimura, Y. Horibe, S.W. Cheong, S. Oh, Phys. Rev. B 84 (2011) 073109.